Illustrative review of cardiac amyloidosis by multimodality imaging

Tanaka, Hidekazu

(Citation)
Heart Failure Reviews,28(1):113-122

(Issue Date)
2023-01

(Resource Type)
journal article

(Version)
Accepted Manuscript

Illustrative review of cardiac amyloidosis by multimodality imaging

Hidekazu Tanaka*

Division of Cardiovascular Medicine, Department of Internal Medicine,

Kobe University Graduate School of Medicine, Kobe, Japan

***Corresponding Author**

Hidekazu Tanaka, MD, PhD, FACC, FASE, FAHA, FESC

Division of Cardiovascular Medicine, Department of Internal Medicine,

Kobe University Graduate School of Medicine, Kobe, Japan

7-5-2, Kusunoki-cho, Chuo-ku, Kobe, 650-0017, Japan

Tel; +81-78-382-5846

Fax; +81-78-382-5859

E-mail; tanakah@med.kobe-u.ac.jp

Abstract

Cardiac involvement in amyloidosis is characterized by the extracellular deposition of misfolded proteins in the heart with the pathognomonic histological property of green birefringence when viewed under cross polarized light after staining with Congo red. Although considered a rare disease, recent data suggest that cardiac amyloidosis is underappreciated as a cause of common cardiac diseases or syndromes. The prognosis for transthyretin (TTR) amyloidosis (ATTR) amyloidosis is better than that for amyloid light-chain amyloidosis, however it is not as good as for other etiologies heart failure. Although there is no proven therapy for patients with ATTR cardiomyopathy (ATTR-CM), tafamidis meglumine, a TTR stabilizer, a study in 2018 found it was associated with reductions in all-cause mortality and cardiovascular-related hospitalizations, as well as with a reduction in the decline in functional capacity and quality of life compared with a placebo for patients with ATTR-CM. As a result of these findings, tafamidis meglumine is currently the only drug approved for patients with both wild-type and variant ATTR-CM, and should be considered for patients whose survival can be reasonably expected. In addition, recent advances in cardiac imaging, diagnostic strategies, and therapies have improved so that interest has been growing in the diagnosis of ATTR-CM by means of non-invasive imaging modalities as a potential means for better management of patients with ATTR-CM. This article reviews the efficacy of non-invasive imaging, especially echocardiography, cardiac magnetic imaging and ^{99m}Tc-pyrophosphate scintigraphy for diagnosis of cardiac amyloidosis.

Key Words: transthyretin cardiac amyloidosis, echocardiography, speckle-tracking echocardiography, global longitudinal strain, cardiac magnetic imaging, ^{99m}Tc-pyrophosphate scintigraphy

Introduction

Amyloidosis is a disease which misfolded proteins form β-sheet structured amyloid fibrils that are deposited in several organs. Amyloidosis is classified as systemic amyloidosis with amyloid deposition in multiple organs, and localized amyloidosis with amyloid deposition in specific organs. It is further classified regarding precursor proteins and their corresponding clinical disease types [1]. Cardiac involvement by amyloidosis is characterized by the extracellular deposition of misfolded proteins in the heart with the pathognomonic histological property of green birefringence when viewed under cross polarized light after staining with Congo red [2]. Of the amyloid fibrils formed by immunoglobulin light chains, transthyretin (TTR), or amyloid A protein (AA) accumulate in the heart, leading cardiac dysfunction. TTR amyloidosis (ATTR) can be either variant ATTR amyloidosis (ATTRv) with a pathogenic mutation in the ATTR gene, or wild-type ATTR amyloidosis (ATTRwt) without any mutation [3]. Current findings indicate that > 98% of diagnosed cardiac amyloidosis forms result from fibrils composed of amyloid light-chain (AL), ATTRv or ATTRwt [4]. Although considered a rare disease, recent data suggest that cardiac amyloidosis is underappreciated as a cause of common cardiac diseases or syndromes [5].

The prognosis of patients with AL amyloidosis is highly dependent on the cardiac involvement and the severity of cardiac damage. According to the Mayo Clinic scoring system using the difference in free light chain, N-terminal pro-brain natriuretic peptide and cardiac troponin T, the median overall survival from diagnosis of patients with stages I, II, III, and IV was 94.1, 40.3, 14, and 5.8 months, respectively[6]. On the other hands, the prognosis for ATTR amyloidosis is better than that for AL amyloidosis, however it is not as good as for other etiologies heart failure (HF).The survival of patients with ATTRwt amyloidosis was thought to be over 60 months [7, 8], but more recent studies suggest that the median survival after diagnosis is only 43-47 months [9, 10]. In addition, the mean life expectancy after diagnosis of ATTRv amyloidosis is approximately 10 years in endemic areas [11], and approximately 7 years for late-onset disease in non-endemic areas [12] when left untreated.

Although there is no proven therapy for patients with ATTR cardiomyopathy (ATTR-CM), tafamidis meglumine, a TTR stabilizer, a study in 2018 found it was associated with reductions in all-cause mortality and cardiovascular-related hospitalizations, as well as with a reduction in the decline in functional capacity and quality of life compared with a placebo for patients with ATTR-CM [12]. As a result of these findings, tafamidis meglumine is currently the only drug approved for patients with both wild-type and variant ATTR-CM, and should be considered for patients whose survival can be reasonably expected [4, 13]. In addition, recent advances in cardiac imaging, diagnostic strategies, and therapies have improved so that interest has been growing in the

diagnosis of ATTR-CM by means of non-invasive imaging modalities as a potential means for better management of patients with ATTR-CM. On the other hands, there is still no proven therapy for patients with AL cardiomyopathy (AL-CM). The aim of treatment for AL amyloidosis is to decrease free-light chain, which is a major cause of toxic amyloid fibrils. The guidelines recommends the combination of cyclophosphamide, bortezomib, and dexamethasone as treatment for both transplant-eligible and transplant-ineligible patients[13].

This article reviews the efficacy of not only echocardiography but also other non-invasive imaging modalities such as cardiac magnetic imaging (CMR), ^{99m}Tc-pyrophosphate (PYP) scintigraphy, amyloid positron emission tomography (PET), and cardiac computed tomography (CT) for diagnosis of cardiac amyloidosis.

Echocardiography

Echocardiography is a non-invasive, easy-to-use reproducible modality for evaluating cardiac morphology and function in cardiac amyloidosis, with some echocardiographic parameters being prognostic for various types of amyloidosis. Conventional echocardiographic features associated with cardiac amyloidosis include concentric left ventricular (LV) hypertrophy (LVH) and right ventricular hypertrophy, normal LV cavity size, dilated atria, and pericardial effusion. Important additional features of conventional echocardiographic features other than LVH include thickened interatrial septum and thickened valves (Fig. 1). LV diastolic dysfunction are generally recognized as the earliest manifestation of cardiac amyloidosis [14], while LV systolic function remains normal until the later stages [15]. Extensive cardiac amyloidosis leads to atrial thrombi, even in patients with sinus rhythm [16], and severe atrial and ventricular amyloid infiltration may also lead to mechanical atrial standstill with eventual thrombus formation [17]. Atrial fibrillation, LV diastolic dysfunction, and lower left atrial appendage velocity have been shown to be independent risk factors for intracardiac thrombosis, whereas anticoagulation has been found to be associated with a significantly decreased risk. The myocardial texture features a distinct “granular sparkling” appearance [18], and it is well known as a key parameter in the diagnosis of cardiac amyloidosis. However, this feature can occur in other causes of LVH, and specificity is as high as 71% - 81%, but sensitivity is as low as 26% - 36% of cardiac amyloidosis cases [19]. It should be noted that “granular sparkling” appearance applies only to standard echocardiographic imaging, without the inclusion of tissue harmonics, as this generally increases myocardial echogenicity. Current echocardiographic image processing techniques may also reduce “granular sparkling” appearance. Thus, the usefulness of “granular sparkling” appearance for diagnosing cardiac amyloidosis is limited.

Cardiac amyloidosis is characterized by an initial impairment of early LV relaxation, whereas HF is associated with impairment of peak systolic wall motion velocities, most prominently seen in the longitudinal myocardial function [20]. Moreover, peak lateral and medial mitral annulus velocities and color M-mode tissue Doppler of the LV posterior wall can differentiate between patients with cardiac amyloidosis and controls with excellent accuracy [21]. Longitudinal myocardial velocity gradients by means of tissue Doppler imaging can indicate differences between the basal- and mid-myocardial velocities, are significantly impaired in HF patients compared with those without [22]. Furthermore, the LV longitudinal myocardial function was found to be impaired in all patients with cardiac amyloidosis compared with only 36% of those with idiopathic restrictive cardiomyopathy [23].

Speckle-tracking strain imaging by echocardiography

While conventional echocardiography is essential for early detection of LV structural abnormalities for cardiac amyloidosis, it has been reported that speckle-tracking strain-derived parameters are useful for early detection of LV structural abnormalities. Especially, global longitudinal strain (GLS) assessed by two-dimensional speckle-tracking imaging is reported as a sensitive marker for early subtle abnormalities of LV myocardial performance, helpful for the prediction of outcomes for various cardiac diseases including various cardiomyopathies, and superior to conventional echocardiographic parameters [24-28]. GLS is determined as the average peak longitudinal strain of 18 LV segments from the standard apical views and can be assessed as a polar plot by ordinary. Polar plot longitudinal strain mapping offers an intuitive visual overview of the global and regional LV longitudinal myocardial functional status of various cardiomyopathies with LVH. It is clinically practicable and the plot patterns obtainable as the result of further developments of this technique in clinical practice provide clues to the etiology of cardiomyopathies, especially for patients with preserved LVEF. It should be noted that cardiac amyloidosis is characterized by regional variations in longitudinal strain from basal segment to apical segment. A preserved longitudinal strain at the apical segments and significantly reduced longitudinal strain at the mid and basal segments is consistently observed [29, 30]. Previous studies have demonstrated that this pattern, known as “Apical Sparing”, is specific, thus suited to differentiate patients with cardiac amyloidosis from patients with other causes of LVH [30, 31]. Phelan et al. compared 55 consecutive patients with cardiac amyloidosis with 30 control subjects with LVH including 15 patients with hypertrophic cardiomyopathy and 15 with aortic stenosis (AS) [29]. A relative apical longitudinal strain of 1.0, which was determined by the formula [average apical longitudinal strain / (average basal-longitudinal strain + mid-longitudinal strain)], was sensitivity of 93% and specificity of 82%

for differentiating patients with cardiac amyloidosis from control patients with LVH with an excellent area under the curve of 0.94. Moreover, Liu et al. showed that a septal apical-to-basal segmental longitudinal strain at a ratio of >2.1 can differentiate cardiac amyloidosis from other causes of concentric LVH with a sensitivity of 88%, specificity of 85% [31]. This specific relative apical sparing can be easily visualized by means of polar plot longitudinal strain mapping for patients with cardiac amyloidosis (Fig. 2). Apical sparing is observed in both patients with ATTR-CM and with AL-CM. However, the strain value at the LV apex of patients with ATTR-CM has been shown to be lower than that of patients with AL-CM [32]. Moreover, Barros-Gomes et al showed that GLS predicted all-cause mortality and provide additional prognostic information for all-cause mortality superior to established clinical, echocardiographic, and serological markers of 150 consecutive patients with AL amyloidosis and preserved LVEF [33]. They also reported that GLS was an independent predictor of all-cause mortality in multivariate Cox regression analysis. Since apical sparing with low GLS would be an important “red flag” for suspected cardiac amyloidosis detected by means of imaging modalities, the speedier diagnosis of ATTR-CM by means of apical sparing may therefore enable earlier administration of tafamidis meglumine.

CMR

CMR is excellent for diagnosing cardiac amyloidosis, and is also useful for differentiating patients with cardiac amyloidosis from those with LVH from other causes. Cardiac amyloidosis is typically diagnosed with cine CMR and late gadolinium enhancement (LGE) on CMR. Cine CMR is a basic sequence for evaluating cardiac morphology and function. Cardiac amyloidosis usually causes LVH, predominantly at the basal segments. The severity of LVH tends to be greater for ATTR-CM than for AL-CM[34]. However, it should be noted that 3-8% of patients with cardiac amyloidosis present with a normal geometry. Thickening of the RV wall and atrial septum is often observed in cardiac amyloidosis, with atrial septum thickening ≥ 6 mm considered to be relatively specific to cardiac amyloidosis [35]. Findings of cine CMR functional analysis indicate that LVEF is often preserved, but may decline as the disease progresses, while advanced cardiac amyloidosis often involves pericardial and pleural effusions [34]. Morphological and functional findings obtained with cine CMR are non-specific, thus making cardiac amyloidosis difficult to diagnose when using this modality alone. LGE imaging is the preferred method for diagnosing cardiac amyloidosis which involves taking images 10 min after the injection of a gadolinium contrast agent to visualize myocardial damage. The diagnostic performance of cardiac amyloidosis with LGE imaging has shown a sensitivity and specificity as high as 85-90% [36, 37]. Typical findings of cardiac amyloidosis on LGE imaging are diffuse LV subendocardial LGE, LGE in the RV wall, LA wall, and

atrial septum, and dark blood pools [38] (Fig. 3). LGE visualizes both amyloid deposition in the myocardial interstitium and subendocardial ischemic changes associated with microangiopathy. LGE patterns tend to be more prominent in ATTR-CM than in AL-CM, and frequently transform into transmural LGE [34]. LGE mostly occurs in the basal segments [39]. LGE transition has been observed from subendocardial to transmural as cardiac amyloidosis progresses while cardiac amyloidosis presents with various atypical LGE patterns depending on the disease stage [40].

Recently, myocardial T1 mapping has been reported to be useful for the quantitative evaluation of myocardial tissue characterization, and is currently recommended for diagnosing cardiac amyloidosis. T1 mapping is an imaging method which quantitatively measures myocardial T1 values. There are two parameters for T1 mapping, that is, native T1, which does not involve use of a contrast agent, and extracellular volume fraction (ECV), which does. Native T1 and ECV frequently yield extremely high values in patients with cardiac amyloidosis[41] (Fig. 4). Native T1 and ECV values for patients with cardiac amyloidosis are reportedly significantly higher than those with other causes of LVH. Sensitivity and specificity for diagnosing cardiac amyloidosis of native T1 range from 80 to 92% and from 56 to 91%, respectively [41, 42], while the corresponding values for diagnosing cardiac amyloidosis of ECV are 93% and 82%, respectively[43]. Cardiac amyloidosis should be strongly suspected when ECV is ≥ 40% [44].

^{99m}Tc-PYP scintigraphy

^{99m}Tc-PYP scintigraphy, a type of bone scintigraphy, features a high capability for diagnosing ATTR-CM. Its use for the diagnosis of ATTR-CM yields a sensitivity of 58-99% and a specificity of 79-100% [45, 46]. However, if false positives, most of which are AL-CM, are excluded, ^{99m}Tc-PYP scintigraphy is considered to have a diagnostic specificity and positive predictive value of 100% [45]. There are two methods for assessment of ^{99m}Tc-PYP scintigraphy for cardiac amyloidosis: visual and quantitative. The basis for both methods is anterior planar imaging [44]. A highly distinguishing trait of ^{99m}Tc-PYP scintigraphy is that, unlike echocardiography and CMR, it can distinguish between AL-CM and ATTR-CM. Visual assessment using 3-h imaging can classify findings as Grade 0 (no cardiac uptake), Grade 1 (mild cardiac uptake, less than rib uptake), Grade 2 (moderate cardiac uptake, equal to rib uptake), and Grade 3 (high cardiac uptake, greater than rib uptake), with Grade 2 and 3 considered positive, with a strong suspicion of ATTR-CM (Fig. 5). Though extremely rare case, there is a patient with ATTR-CM without cardiac uptake by ^{99m}Tc-PYP scintigraphy (Fig. 6).

Recent topics of interest include the finding that substantial percentages of patients with ATTR-CM can be found among those with HF with preserved ejection fraction (HFpEF) and those

with AS who have been referred for transcatheter aortic valve replacement (TAVR). It was found that 13-14% of patients with HFpEF were accounted for by those with ATTR-CM [47, 48], and for 12-16% of patients with severe AS who had been referred for TAVR [49, 50]. A recent study has assessed the utility of ^{99m}Tc-PYP scintigraphy for screening of patients with ATTR-CM from among those with HFpEF or AS based on a non-biopsy diagnosis. Fig. 7 shows a case with ATTRwt-CM manifesting as HFpEF, although conventional echocardiographic findings did not unequivocally indicate typical cardiac amyloidosis. However, the presence of apical sparing based on ^{99m}Tc-PYP scintigraphic findings led to an early diagnosis of ATTRwt-CM followed by an early intervention using tafamidis meglumine. Since there is currently no established medical treatment for patients with HFpEF, early diagnosis of ATTR-CM patients among those with HFpEF plays an important role in treatment by means of tafamidis meglumine. Another case, shown in Fig. 8, shows findings for a patient with severe AS who was scheduled for TAVR as treatment for being complicated with ATTRwt-CM. Similar to the case in Fig. 7, the presence of apical sparing based on ^{99m}Tc-PYP scintigraphic findings led to a diagnosis of ATTRwt-CM. This patient received tafamidis meglumine after TAVR. Given the high prevalence of AS in the general population and the increasing frequency of the use of TAVR for older adults at high and intermediate surgical risk, and the fact that more than half of HF patients are currently HFpEF, ^{99m}Tc-PYP scintigraphy has proven to be an effective screening tool for ATTR-CA among AS patients scheduled to undergo TAVR and HFpEF. Screening for ATTR-CA may result in early identification of ATTR-CA cases of severe AS and/or HFpEF when emerging therapies may be of greater benefit.

Amyloid PET

The application of amyloid PET in patients with cardiac amyloidosis has been the subject of pre-clinical research reports. Myocardial uptake of ^{11}C-Pittsburgh compound B[51], ^{18}F-florbetapir[52], and ^{18}F-florbetaben[53] has been confirmed for both patients with AL-CM and ATTR-CM, and has been shown to be significantly higher in such patients compared with controls. The cardiac uptake of ^{18}F-florbetapir and ^{18}F-florbetaben tends to be higher in patients with AL-CM than in those with ATTR-CM. Amyloid PET is also used to assess amyloid deposition not only in the heart, but also in the whole body. Thus, amyloid PET can be capable of quantifying amyloid deposition in the whole body.

Cardiac CT

Cardiac CT can be used as an alternative to CMR for assessing myocardial late enhancement and ECV. Myocardial contrast enhancement or iodine density values can be used to

calculate ECV in late enhancement CT and assess it in a manner comparable to CMR T1 mapping[54, 55]. Cardiac CT-derived ECV is significantly higher in cardiac amyloidosis similar to CMR, and suited to differentiate patients with cardiac amyloidosis from those with other causes of LVH. Scully et al reported that patients with cardiac CT-derived ECV ≥ 31% were suspected of cardiac amyloidosis from 109 patients with severe AS who underwent ^{99m}Tc-PYP scintigraphy and routine TAVR evaluation CT imaging[56]. As described previously, substantial percentages of patients with ATTR-CM can be found among those with severe AS who have been referred for TAVR. Since patients with AS who are scheduled TAVR usually undergo cardiac CT, cardiac CT has the advantage that both indication of TAVR and the assessment of ATTR-CM can be evaluated simultaneously for such patients (Fig. 9).

Conclusions

Cardiac amyloidosis is an inexorably progressive and eventually fatal cardiomyopathy associated with poor quality of life. Although diagnosis is often delayed for many years after symptoms develop, improved awareness and wider use of recently validated diagnostic imaging methods, especially echocardiography is urgently required so that such patients may benefit from recent therapeutic developments.

Acknowledgments

I thank Dr, Takayoshi Toba and Yu Izawa in the Kobe University Hospital for the support of CMR, ^{99m}Tc-PYP scintigraphy, and cardiac CT.

Figure Legends

Fig. 1: Examples of apical 4-chamber views of wild-type transthyretin amyloid cardiomyopathy, showing a thickened interatrial septum and thickened mitral valve as well as left ventricular and right ventricular hypertrophy.

Fig. 2: Examples of parasternal long-axis views and longitudinal strain bull's eye plots for patients with left ventricular hypertrophy including a patient with wild-type transthyretin amyloid cardiomyopathy (ATTRwt-CM), hypertrophic cardiomyopathy and severe aortic stenosis. Global longitudinal strain (GLS) for all three patients is low, but an apical sparing pattern in the patient with ATTRwt-CM can be seen (arrow).

Fig. 3: Examples of late gadolinium enhancement (LGE) obtained with cardiac magnetic imaging (CMR) for a patient with wild-type transthyretin amyloid cardiomyopathy, showing diffuse left ventricular subendocardial (white arrow), left atrial wall (white dotted arrow), and interatrial septum LGE (red arrow).

Fig. 4: Examples of T1 mapping obtained with CMR for a patient with wild-type transthyretin amyloid cardiomyopathy (ATTRwt-CM) and hypertrophic cardiomyopathy, demonstrating that the native T1 value in a patient with ATTRwt-CM is extremely high and abnormally value.

Fig. 5: Examples of the parasternal long-axis view and ^{99m}Tc-pyrophosphate (PYP) scintigraphy for patients with left ventricular hypertrophy, one patient with essential hypertension, one with amyloid light-chain amyloid cardiomyopathy (AL-CM), and one with wild-type transthyretin amyloid cardiomyopathy (ATTRwt-CM). Grade 3 cardiac uptake was observed in ATTRwt-CM

Fig. 6: Examples of the parasternal long-axis view, 12-lead electrocardiogram, and ^{99m}Tc-pyrophosphate (PYP) scintigraphy for a patient with transthyretin amyloid cardiomyopathy who was hospitalized with acute heart failure. The patient had low voltage on 12-lead electrocardiogram despite left ventricular hypertrophy, but ^{99m}Tc-PYP scintigraphy shows Grade 0 cardiac uptake. However, the patient was diagnosed as transthyretin amyloid cardiomyopathy by postmortem examination.
IVST, interventricular septum thickness; PWT, posterior wall thickness; LVEDV, left ventricular end-diastolic volume; LVESV, left ventricular end-systolic volume; LVEF, left ventricular ejection fraction; LAVI, left atrial volume index.

Fig. 7: Examples of the parasternal long-axis view, apical 4-chamber view, Doppler-derived LV diastolic filling, longitudinal strain bull's eye plot and ^{99m}Tc-pyrophosphate (PYP) scintigraphy for a patient with wild-type transthyretin amyloid cardiomyopathy who was hospitalized with acute heart failure due to heart failure with preserved ejection fraction. Global longitudinal strain (GLS) of 13.0% is low, but an apical sparing pattern can be observed. Moreover, ^{99m}Tc-PYP scintigraphy shows Grade 3 cardiac uptake.
IVST, interventricular septum thickness; PWT, posterior wall thickness; LVEDV, left ventricular end-diastolic volume; LVESV, left ventricular end-systolic volume; LVEF, left ventricular ejection fraction; LAVI, left atrial volume index.

Fig. 8: Examples of the parasternal long-axis view, longitudinal strain bull's eye plot and ^{99m}Tc-pyrophosphate (PYP) scintigraphy for a patient with severe aortic stenosis who was referred for transcatheter aortic valve implantation complicated with wild-type transthyretin amyloid cardiomyopathy. Although global longitudinal strain (GLS) of 9.8% is low, an apical sparing pattern can be observed. Moreover, ^{99m}Tc-PYP scintigraphy shows Grade 3 cardiac uptake.
IVST, interventricular septum thickness; PWT, posterior wall thickness; LVEDV, left ventricular end-diastolic volume; LVESV, left ventricular end-systolic volume; LVEF, left ventricular ejection fraction; LAVI, left atrial volume index.

Fig. 9: Examples of the parasternal long-axis view, cardiac computed tomography (CT) and ^{99m}Tc-pyrophosphate (PYP) scintigraphy for a patient with severe aortic stenosis who was referred for transcatheter aortic valve implantation complicated with wild-type transthyretin amyloid cardiomyopathy. Since cardiac CT-derived extracellular volume fraction (ECV) is as high as 34%, ^{99m}Tc-PYP scintigraphy was performed (Grade 2 cardiac uptake).
IVST, interventricular septum thickness; PWT, posterior wall thickness; LVEDV, left ventricular end-diastolic volume; LVESV, left ventricular end-systolic volume; LVEF, left ventricular ejection fraction; LAVI, left atrial volume index.

References

1. Benson MD, Buxbaum JN, Eisenberg DS, Merlini G, Saraiva MJM, Sekijima Y, Sipe JD, Westermark P (2018) Amyloid nomenclature 2018: recommendations by the International Society of Amyloidosis (ISA) nomenclature committee. Amyloid 25(4) 215-219. 10.1080/13506129.2018.1549825

2. Maurer MS, Elliott P, Comenzo R, Semigran M, Rapezzi C (2017) Addressing Common Questions Encountered in the Diagnosis and Management of Cardiac Amyloidosis. Circulation 135(14) 1357-1377. 10.1161/CIRCULATIONAHA.116.024438

3. Wechalekar AD, Gillmore JD, Hawkins PN (2016) Systemic amyloidosis. Lancet 387(10038) 2641-2654. 10.1016/S0140-6736(15)01274-X

4. Garcia-Pavia P, Rapezzi C, Adler Y, Arad M, Basso C, Brucato A, Burazor I, Caforio ALP, Damy T, Eriksson U, Fontana M, Gillmore JD, Gonzalez-Lopez E, Grogan M, Heymans S, Imazio M, Kindermann I, Kristen AV, Maurer MS, Merlini G, Pantazis A, Pankuweit S, Rigopoulos AG, Linhart A (2021) Diagnosis and treatment of cardiac amyloidosis: a position statement of the ESC Working Group on Myocardial and Pericardial Diseases. Eur Heart J 42(16) 1554-1568. 10.1093/eurheartj/ehab072

5. Ruberg FL, Grogan M, Hanna M, Kelly JW, Maurer MS (2019) Transthyretin Amyloid

Cardiomyopathy: JACC State-of-the-Art Review. J Am Coll Cardiol 73(22) 2872-2891. 10.1016/j.jacc.2019.04.003

6. Kumar S, Dispenzieri A, Lacy MQ, Hayman SR, Buadi FK, Colby C, Laumann K, Zeldenrust SR, Leung N, Dingli D, Greipp PR, Lust JA, Russell SJ, Kyle RA, Rajkumar SV, Gertz MA (2012) Revised prognostic staging system for light chain amyloidosis incorporating cardiac biomarkers and serum free light chain measurements. J Clin Oncol 30(9) 989-995. 10.1200/JCO.2011.38.5724

7. Kyle RA, Spittell PC, Gertz MA, Li CY, Edwards WD, Olson LJ, Thibodeau SN (1996) The premortem recognition of systemic senile amyloidosis with cardiac involvement. Am J Med 101(4) 395-400. 10.1016/S0002-9343(96)00229-X

8. Ng B, Connors LH, Davidoff R, Skinner M, Falk RH (2005) Senile systemic amyloidosis presenting with heart failure: a comparison with light chain-associated amyloidosis. Arch Intern Med 165(12) 1425-1429. 10.1001/archinte.165.12.1425

9. Connors LH, Sam F, Skinner M, Salinaro F, Sun F, Ruberg FL, Berk JL, Seldin DC (2016) Heart Failure Resulting From Age-Related Cardiac Amyloid Disease Associated With Wild-Type Transthyretin: A Prospective, Observational Cohort Study. Circulation 133(3) 282-290. 10.1161/CIRCULATIONAHA.115.018852

10. Grogan M, Scott CG, Kyle RA, Zeldenrust SR, Gertz MA, Lin G, Klarich KW, Miller WL, Maleszewski JJ, Dispenzieri A (2016) Natural History of Wild-Type Transthyretin Cardiac Amyloidosis and Risk Stratification Using a Novel Staging System. J Am Coll Cardiol 68(10) 1014-1020. 10.1016/j.jacc.2016.06.033

11. Yamashita T, Ando Y, Okamoto S, Misumi Y, Hirahara T, Ueda M, Obayashi K, Nakamura M, Jono H, Shono M, Asonuma K, Inomata Y, Uchino M (2012) Long-term survival after liver transplantation in patients with familial amyloid polyneuropathy. Neurology 78(9) 637-643. 10.1212/WNL.0b013e318248df18

12. Koike H, Tanaka F, Hashimoto R, Tomita M, Kawagashira Y, Iijima M, Fujitake J, Kawanami T, Kato T, Yamamoto M, Sobue G (2012) Natural history of transthyretin Val30Met familial amyloid polyneuropathy: analysis of late-onset cases from non-endemic areas. J Neurol Neurosurg Psychiatry 83(2) 152-158. 10.1136/jnnp-2011-301299

13. Wechalekar AD, Gillmore JD, Bird J, Cavenagh J, Hawkins S, Kazmi M, Lachmann HJ, Hawkins PN, Pratt G, Committee B (2015) Guidelines on the management of AL amyloidosis. Br J Haematol 168(2) 186-206. 10.1111/bjh.13155

14. Klein AL, Hatle LK, Taliercio CP, Taylor CL, Kyle RA, Bailey KR, Seward JB, Tajik AJ (1990) Serial Doppler echocardiographic follow-up of left ventricular diastolic function in cardiac

amyloidosis. J Am Coll Cardiol 16(5) 1135-1141. 10.1016/0735-1097(90)90545-z

15. Swanton RH, Brooksby IA, Davies MJ, Coltart DJ, Jenkins BS, Webb-Peploe MM (1977) Systolic and diastolic ventricular function in cardiac amyloidosis. Studies in six cases diagnosed with endomyocardial biopsy. Am J Cardiol 39(5) 658-664. 10.1016/s0002-9149(77)80125-2

16. Dubrey S, Pollak A, Skinner M, Falk RH (1995) Atrial thrombi occurring during sinus rhythm in cardiac amyloidosis: evidence for atrial electromechanical dissociation. Br Heart J 74(5) 541-544. 10.1136/hrt.74.5.541

17. Feng D, Syed IS, Martinez M, Oh JK, Jaffe AS, Grogan M, Edwards WD, Gertz MA, Klarich KW (2009) Intracardiac thrombosis and anticoagulation therapy in cardiac amyloidosis. Circulation 119(18) 2490-2497. 10.1161/CIRCULATIONAHA.108.785014

18. Siqueira-Filho AG, Cunha CL, Tajik AJ, Seward JB, Schattenberg TT, Giuliani ER (1981) M-mode and two-dimensional echocardiographic features in cardiac amyloidosis. Circulation 63(1) 188-196. 10.1161/01.cir.63.1.188

19. Selvanayagam JB, Hawkins PN, Paul B, Myerson SG, Neubauer S (2007) Evaluation and management of the cardiac amyloidosis. J Am Coll Cardiol 50(22) 2101-2110. 10.1016/j.jacc.2007.08.028

20. Koyama J, Ray-Sequin PA, Davidoff R, Falk RH (2002) Usefulness of pulsed tissue Doppler imaging for evaluating systolic and diastolic left ventricular function in patients with AL (primary) amyloidosis. Am J Cardiol 89(9) 1067-1071. 10.1016/s0002-9149(02)02277-4

21. Palka P, Lange A, Donnelly JE, Scalia G, Burstow DJ, Nihoyannopoulos P (2002) Doppler tissue echocardiographic features of cardiac amyloidosis. J Am Soc Echocardiogr 15(11) 1353-1360. 10.1067/mje.2002.125285

22. Koyama J, Davidoff R, Falk RH (2004) Longitudinal myocardial velocity gradient derived from pulsed Doppler tissue imaging in AL amyloidosis: a sensitive indicator of systolic and diastolic dysfunction. J Am Soc Echocardiogr 17(1) 36-44. 10.1016/j.echo.2003.09.014

23. Perugini E, Rapezzi C, Reggiani LB, Poole-Wilson P, Branzi A, Henein MY (2005) Comparison of ventricular long-axis function in patients with cardiac amyloidosis versus idiopathic restrictive cardiomyopathy. Am J Cardiol 95(1) 146-149. 10.1016/j.amjcard.2004.08.084

24. Tanaka H (2019) Utility of strain imaging in conjunction with heart failure stage classification for heart failure patient management. J Echocardiogr 17(1) 17-24. 10.1007/s12574-018-0408-2

25. Tanaka H (2021) Efficacy of echocardiography for differential diagnosis of left ventricular

hypertrophy: special focus on speckle-tracking longitudinal strain. J Echocardiogr 19(2) 71-79. 10.1007/s12574-020-00508-3

26. Gorcsan J, 3rd, Tanaka H (2011) Echocardiographic assessment of myocardial strain. J Am Coll Cardiol 58(14) 1401-1413. 10.1016/j.jacc.2011.06.038

27. Biering-Sorensen T, Biering-Sorensen SR, Olsen FJ, Sengelov M, Jorgensen PG, Mogelvang R, Shah AM, Jensen JS (2017) Global Longitudinal Strain by Echocardiography Predicts Long-Term Risk of Cardiovascular Morbidity and Mortality in a Low-Risk General Population: The Copenhagen City Heart Study. Circ Cardiovasc Imaging 10(3) 10.1161/CIRCIMAGING.116.005521

28. Stanton T, Leano R, Marwick TH (2009) Prediction of all-cause mortality from global longitudinal speckle strain: comparison with ejection fraction and wall motion scoring. Circ Cardiovasc Imaging 2(5) 356-364. 10.1161/CIRCIMAGING.109.862334

29. Phelan D, Collier P, Thavendiranathan P, Popovic ZB, Hanna M, Plana JC, Marwick TH, Thomas JD (2012) Relative apical sparing of longitudinal strain using two-dimensional speckle-tracking echocardiography is both sensitive and specific for the diagnosis of cardiac amyloidosis. Heart 98(19) 1442-1448. 10.1136/heartjnl-2012-302353

30. Liu D, Hu K, Niemann M, Herrmann S, Cikes M, Stork S, Beer M, Gaudron PD, Morbach

C, Knop S, Geissinger E, Ertl G, Bijnens B, Weidemann F (2013) Impact of regional left ventricular function on outcome for patients with AL amyloidosis. PLoS One 8(3) e56923. 10.1371/journal.pone.0056923

31. Liu D, Hu K, Niemann M, Herrmann S, Cikes M, Stork S, Gaudron PD, Knop S, Ertl G, Bijnens B, Weidemann F (2013) Effect of combined systolic and diastolic functional parameter assessment for differentiation of cardiac amyloidosis from other causes of concentric left ventricular hypertrophy. Circ Cardiovasc Imaging 6(6) 1066-1072. 10.1161/CIRCIMAGING.113.000683

32. Tuzovic M, Yang EH, Baas AS, Depasquale EC, Deng MC, Cruz D, Vorobiof G (2017) Cardiac Amyloidosis: Diagnosis and Treatment Strategies. Curr Oncol Rep 19(7) 46. 10.1007/s11912-017-0607-4

33. Barros-Gomes S, Williams B, Nhola LF, Grogan M, Maalouf JF, Dispenzieri A, Pellikka PA, Villarraga HR (2017) Prognosis of Light Chain Amyloidosis With Preserved LVEF: Added Value of 2D Speckle-Tracking Echocardiography to the Current Prognostic Staging System. JACC Cardiovasc Imaging 10(4) 398-407. 10.1016/j.jcmg.2016.04.008

34. Dungu JN, Valencia O, Pinney JH, Gibbs SD, Rowczenio D, Gilbertson JA, Lachmann HJ, Wechalekar A, Gillmore JD, Whelan CJ, Hawkins PN, Anderson LJ (2014) CMR-based differentiation of AL and ATTR cardiac amyloidosis. JACC Cardiovasc Imaging 7(2) 133-142.

10.1016/j.jcmg.2013.08.015

35. Fattori R, Rocchi G, Celletti F, Bertaccini P, Rapezzi C, Gavelli G (1998) Contribution of magnetic resonance imaging in the differential diagnosis of cardiac amyloidosis and symmetric hypertrophic cardiomyopathy. Am Heart J 136(5) 824-830. 10.1016/s0002-8703(98)70127-9

36. Martinez-Naharro A, Treibel TA, Abdel-Gadir A, Bulluck H, Zumbo G, Knight DS, Kotecha T, Francis R, Hutt DF, Rezk T, Rosmini S, Quarta CC, Whelan CJ, Kellman P, Gillmore JD, Moon JC, Hawkins PN, Fontana M (2017) Magnetic Resonance in Transthyretin Cardiac Amyloidosis. J Am Coll Cardiol 70(4) 466-477. 10.1016/j.jacc.2017.05.053

37. Maceira AM, Prasad SK, Hawkins PN, Roughton M, Pennell DJ (2008) Cardiovascular magnetic resonance and prognosis in cardiac amyloidosis. J Cardiovasc Magn Reson 10(54. 10.1186/1532-429X-10-54

38. Syed IS, Glockner JF, Feng D, Araoz PA, Martinez MW, Edwards WD, Gertz MA, Dispenzieri A, Oh JK, Bellavia D, Tajik AJ, Grogan M (2010) Role of cardiac magnetic resonance imaging in the detection of cardiac amyloidosis. JACC Cardiovasc Imaging 3(2) 155-164. 10.1016/j.jcmg.2009.09.023

39. Wan K, Sun J, Yang D, Liu H, Wang J, Cheng W, Zhang Q, Zeng Z, Zhang T, Greiser A,

Jolly MP, Han Y, Chen Y (2018) Left Ventricular Myocardial Deformation on Cine MR Images: Relationship to Severity of Disease and Prognosis in Light-Chain Amyloidosis. Radiology 288(1) 73-80. 10.1148/radiol.2018172435

40. Fontana M, Pica S, Reant P, Abdel-Gadir A, Treibel TA, Banypersad SM, Maestrini V, Barcella W, Rosmini S, Bulluck H, Sayed RH, Patel K, Mamhood S, Bucciarelli-Ducci C, Whelan CJ, Herrey AS, Lachmann HJ, Wechalekar AD, Manisty CH, Schelbert EB, Kellman P, Gillmore JD, Hawkins PN, Moon JC (2015) Prognostic Value of Late Gadolinium Enhancement Cardiovascular Magnetic Resonance in Cardiac Amyloidosis. Circulation 132(16) 1570-1579. 10.1161/CIRCULATIONAHA.115.016567

41. Fontana M, Banypersad SM, Treibel TA, Maestrini V, Sado DM, White SK, Pica S, Castelletti S, Piechnik SK, Robson MD, Gilbertson JA, Rowczenio D, Hutt DF, Lachmann HJ, Wechalekar AD, Whelan CJ, Gillmore JD, Hawkins PN, Moon JC (2014) Native T1 mapping in transthyretin amyloidosis. JACC Cardiovasc Imaging 7(2) 157-165. 10.1016/j.jcmg.2013.10.008

42. Karamitsos TD, Piechnik SK, Banypersad SM, Fontana M, Ntusi NB, Ferreira VM, Whelan CJ, Myerson SG, Robson MD, Hawkins PN, Neubauer S, Moon JC (2013) Noncontrast T1 mapping for the diagnosis of cardiac amyloidosis. JACC Cardiovasc Imaging 6(4) 488-497. 10.1016/j.jcmg.2012.11.013

43. Martinez-Naharro A, Kotecha T, Norrington K, Boldrini M, Rezk T, Quarta C, Treibel TA, Whelan CJ, Knight DS, Kellman P, Ruberg FL, Gillmore JD, Moon JC, Hawkins PN, Fontana M (2019) Native T1 and Extracellular Volume in Transthyretin Amyloidosis. JACC Cardiovasc Imaging 12(5) 810-819. 10.1016/j.jcmg.2018.02.006

44. Dorbala S, Ando Y, Bokhari S, Dispenzieri A, Falk RH, Ferrari VA, Fontana M, Gheysens O, Gillmore JD, Glaudemans A, Hanna MA, Hazenberg BPC, Kristen AV, Kwong RY, Maurer MS, Merlini G, Miller EJ, Moon JC, Murthy VL, Quarta CC, Rapezzi C, Ruberg FL, Shah SJ, Slart R, Verberne HJ, Bourque JM (2019) ASNC/AHA/ASE/EANM/HFSA/ISA/SCMR/SNMMI expert consensus recommendations for multimodality imaging in cardiac amyloidosis: Part 1 of 2-evidence base and standardized methods of imaging. J Nucl Cardiol 26(6) 2065-2123. 10.1007/s12350-019-01760-6

45. Gillmore JD, Maurer MS, Falk RH, Merlini G, Damy T, Dispenzieri A, Wechalekar AD, Berk JL, Quarta CC, Grogan M, Lachmann HJ, Bokhari S, Castano A, Dorbala S, Johnson GB, Glaudemans AW, Rezk T, Fontana M, Palladini G, Milani P, Guidalotti PL, Flatman K, Lane T, Vonberg FW, Whelan CJ, Moon JC, Ruberg FL, Miller EJ, Hutt DF, Hazenberg BP, Rapezzi C, Hawkins PN (2016) Nonbiopsy Diagnosis of Cardiac Transthyretin Amyloidosis. Circulation 133(24) 2404-2412. 10.1161/CIRCULATIONAHA.116.021612

46. Castano A, Haq M, Narotsky DL, Goldsmith J, Weinberg RL, Morgenstern R, Pozniakoff T, Ruberg FL, Miller EJ, Berk JL, Dispenzieri A, Grogan M, Johnson G, Bokhari S, Maurer MS (2016) Multicenter Study of Planar Technetium 99m Pyrophosphate Cardiac Imaging: Predicting Survival for Patients With ATTR Cardiac Amyloidosis. JAMA Cardiol 1(8) 880-889. 10.1001/jamacardio.2016.2839

47. Hahn VS, Yanek LR, Vaishnav J, Ying W, Vaidya D, Lee YZJ, Riley SJ, Subramanya V, Brown EE, Hopkins CD, Ononogbu S, Perzel Mandell K, Halushka MK, Steenbergen C, Jr., Rosenberg AZ, Tedford RJ, Judge DP, Shah SJ, Russell SD, Kass DA, Sharma K (2020) Endomyocardial Biopsy Characterization of Heart Failure With Preserved Ejection Fraction and Prevalence of Cardiac Amyloidosis. JACC Heart Fail 8(9) 712-724. 10.1016/j.jchf.2020.04.007

48. Gonzalez-Lopez E, Gallego-Delgado M, Guzzo-Merello G, de Haro-Del Moral FJ, Cobo-Marcos M, Robles C, Bornstein B, Salas C, Lara-Pezzi E, Alonso-Pulpon L, Garcia-Pavia P (2015) Wild-type transthyretin amyloidosis as a cause of heart failure with preserved ejection fraction. Eur Heart J 36(38) 2585-2594. 10.1093/eurheartj/ehv338

49. Castano A, Narotsky DL, Hamid N, Khalique OK, Morgenstern R, DeLuca A, Rubin J, Chiuzan C, Nazif T, Vahl T, George I, Kodali S, Leon MB, Hahn R, Bokhari S, Maurer MS (2017) Unveiling transthyretin cardiac amyloidosis and its predictors among elderly patients with severe

aortic stenosis undergoing transcatheter aortic valve replacement. Eur Heart J 38(38) 2879-2887. 10.1093/eurheartj/ehx350

50. Nitsche C, Scully PR, Patel KP, Kammerlander AA, Koschutnik M, Dona C, Wollenweber T, Ahmed N, Thornton GD, Kelion AD, Sabharwal N, Newton JD, Ozkor M, Kennon S, Mullen M, Lloyd G, Fontana M, Hawkins PN, Pugliese F, Menezes LJ, Moon JC, Mascherbauer J, Treibel TA (2021) Prevalence and Outcomes of Concomitant Aortic Stenosis and Cardiac Amyloidosis. J Am Coll Cardiol 77(2) 128-139. 10.1016/j.jacc.2020.11.006

51. Lee SP, Lee ES, Choi H, Im HJ, Koh Y, Lee MH, Kwon JH, Paeng JC, Kim HK, Cheon GJ, Kim YJ, Kim I, Yoon SS, Seo JW, Sohn DW (2015) 11C-Pittsburgh B PET imaging in cardiac amyloidosis. JACC Cardiovasc Imaging 8(1) 50-59. 10.1016/j.jcmg.2014.09.018

52. Park MA, Padera RF, Belanger A, Dubey S, Hwang DH, Veeranna V, Falk RH, Di Carli MF, Dorbala S (2015) 18F-Florbetapir Binds Specifically to Myocardial Light Chain and Transthyretin Amyloid Deposits: Autoradiography Study. Circ Cardiovasc Imaging 8(8) 10.1161/CIRCIMAGING.114.002954

53. Law WP, Wang WY, Moore PT, Mollee PN, Ng AC (2016) Cardiac Amyloid Imaging with 18F-Florbetaben PET: A Pilot Study. J Nucl Med 57(11) 1733-1739. 10.2967/jnumed.115.169870

54. Bandula S, White SK, Flett AS, Lawrence D, Pugliese F, Ashworth MT, Punwani S, Taylor SA, Moon JC (2013) Measurement of myocardial extracellular volume fraction by using equilibrium contrast-enhanced CT: validation against histologic findings. Radiology 269(2) 396-403. 10.1148/radiol.13130130

10.1148/radiology.13130130

55. Oda S, Emoto T, Nakaura T, Kidoh M, Utsunomiya D, Funama Y, Nagayama Y, Takashio S, Ueda M, Yamashita T, Tsujita K, Ando Y, Yamashita Y (2019) Myocardial Late Iodine Enhancement and Extracellular Volume Quantification with Dual-Layer Spectral Detector Dual-Energy Cardiac CT. Radiol Cardiothorac Imaging 1(1) e180003. 10.1148/ryct.2019180003

56. Scully PR, Patel KP, Saberwal B, Klotz E, Augusto JB, Thornton GD, Hughes RK, Manisty C, Lloyd G, Newton JD, Sabharwal N, Kelion A, Kennon S, Ozkor M, Mullen M, Hartman N, Cavalcante JL, Menezes LJ, Hawkins PN, Treibel TA, Moon JC, Pugliese F (2020) Identifying Cardiac Amyloid in Aortic Stenosis: ECV Quantification by CT in TAVR Patients. JACC Cardiovasc Imaging 13(10) 2177-2189. 10.1016/j.jcmg.2020.05.029

Figure 1

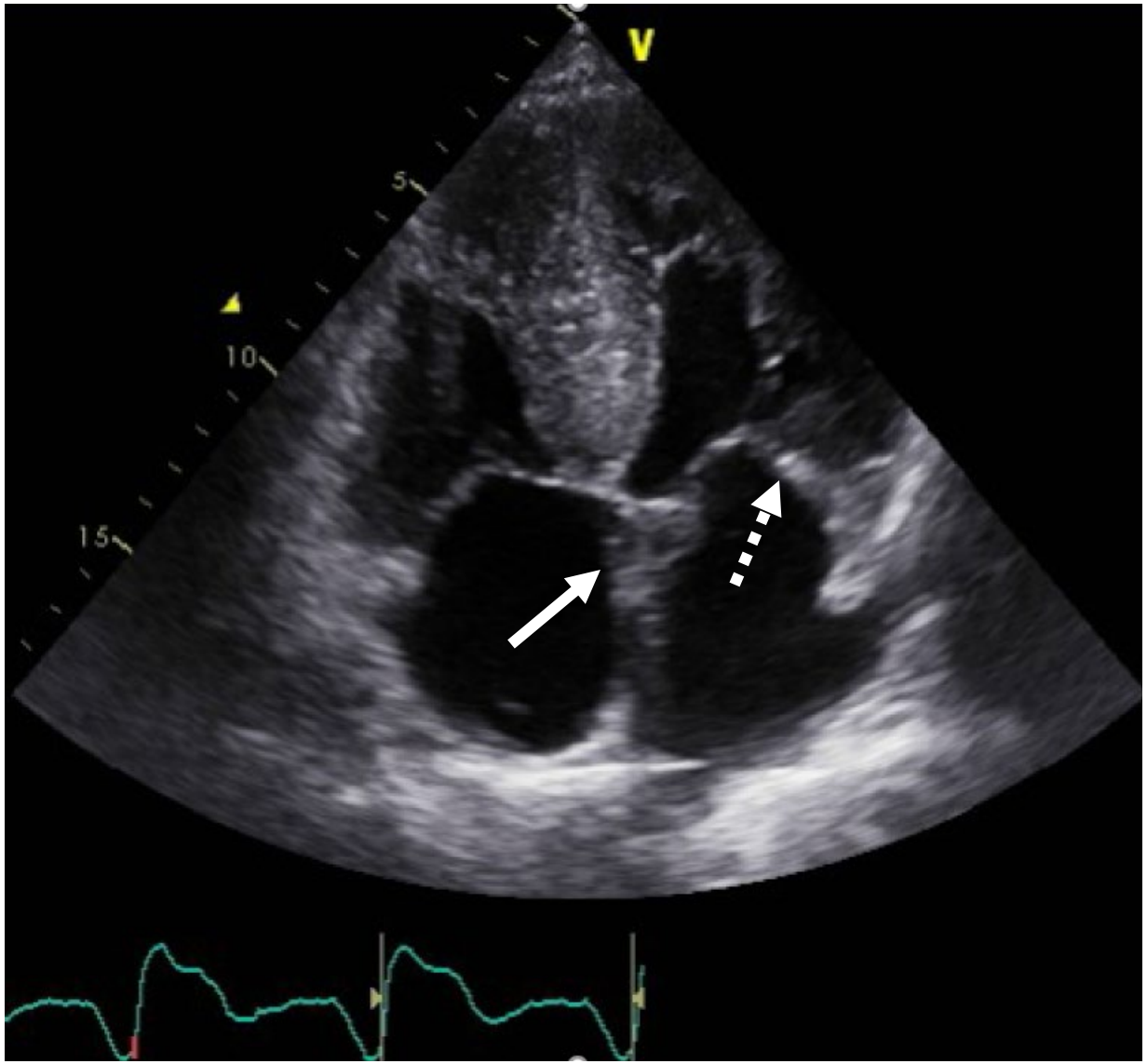

Figure 2

ATTRwt-CM

Parasternal long-axis view

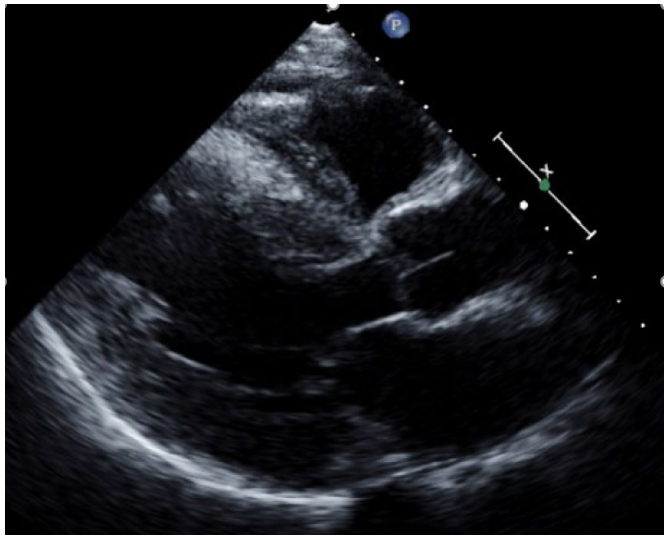

Polar Plot Longitudinal Strain Mapping

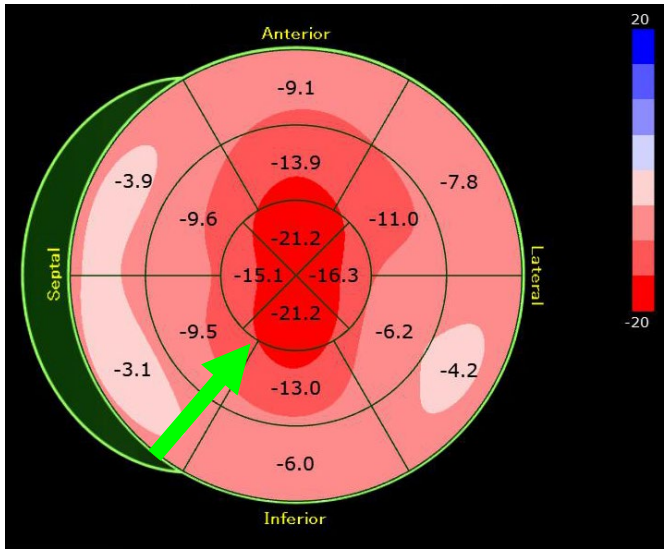

GLS=14.2%

Hypertrophic Cardiomyopathy

Parasternal long-axis view

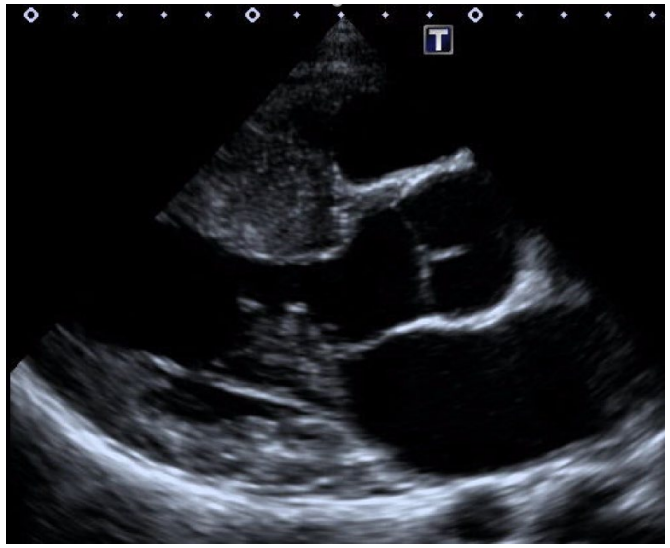

Polar Plot Longitudinal Strain Mapping

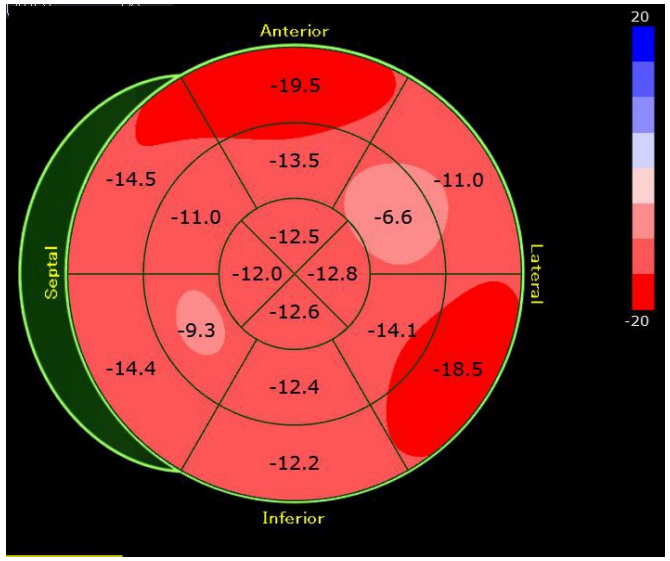

GLS=13.2%

Aortic Stenosis

Parasternal long-axis view

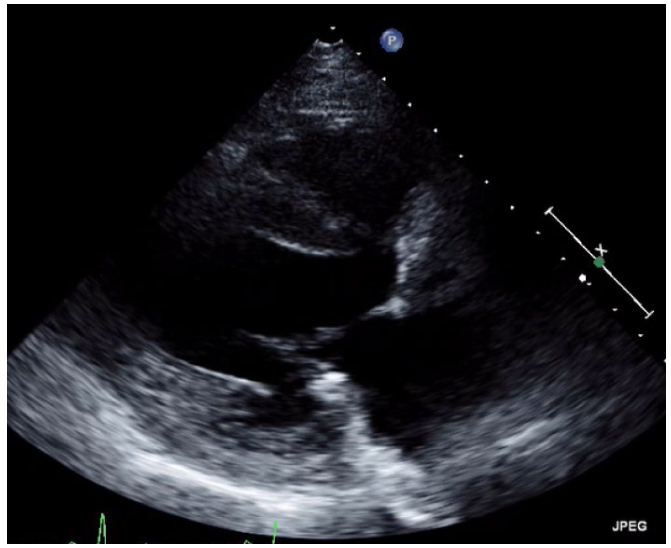

Polar Plot Longitudinal Strain Mapping

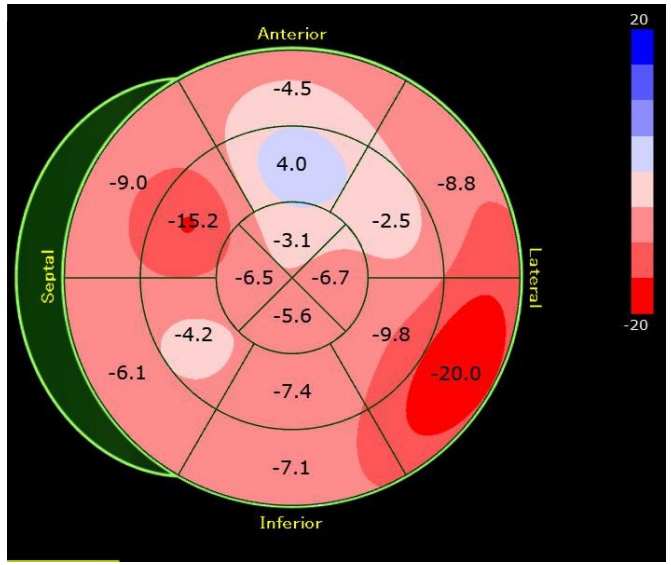

GLS=8.9%

Figure 3

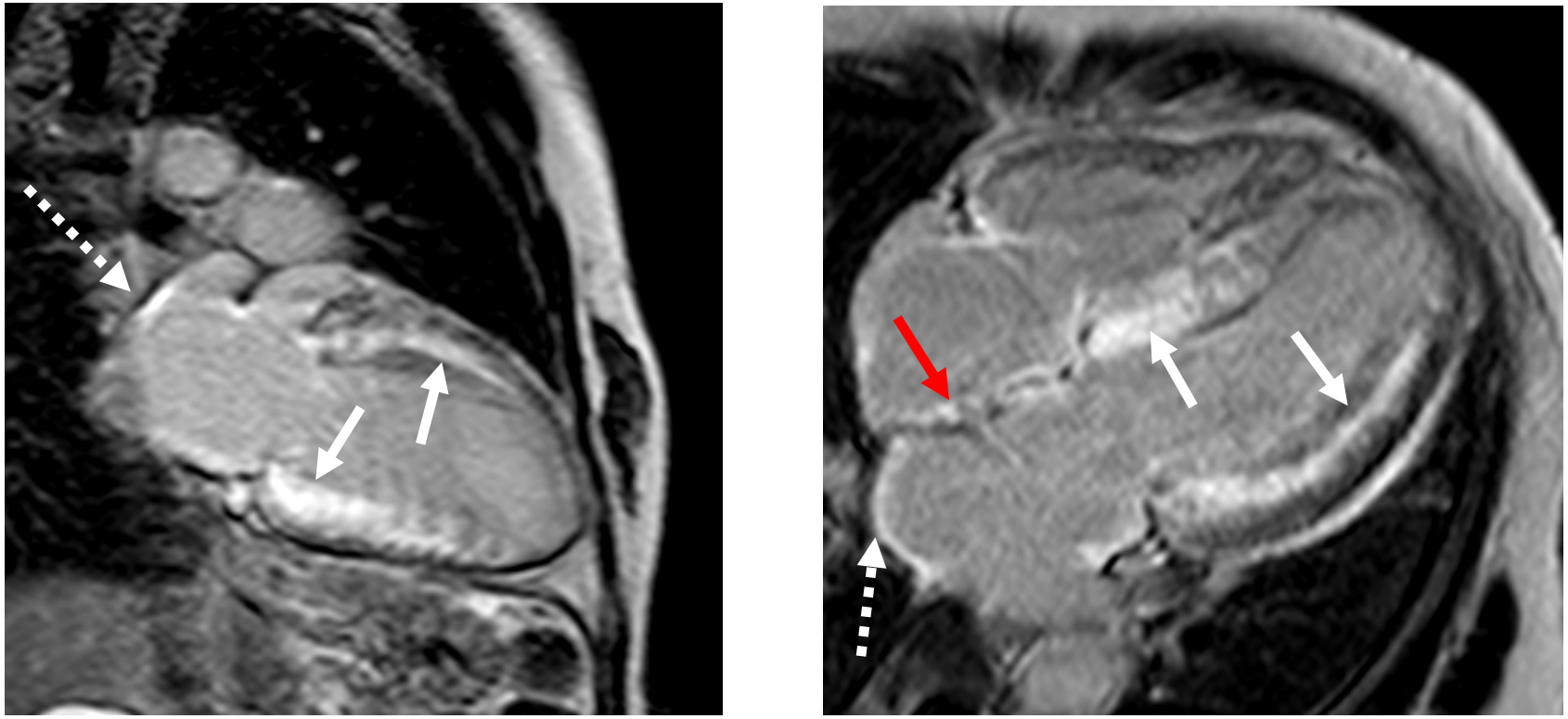

Figure 4

ATTRwt-CM

Parasternal long-axis view

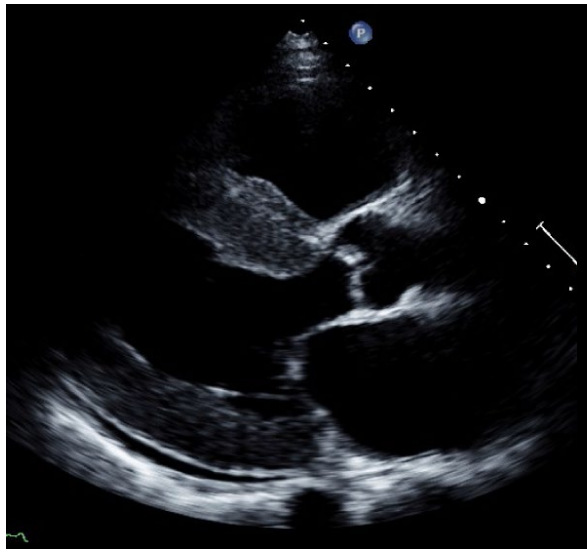

CMR T1 mapping

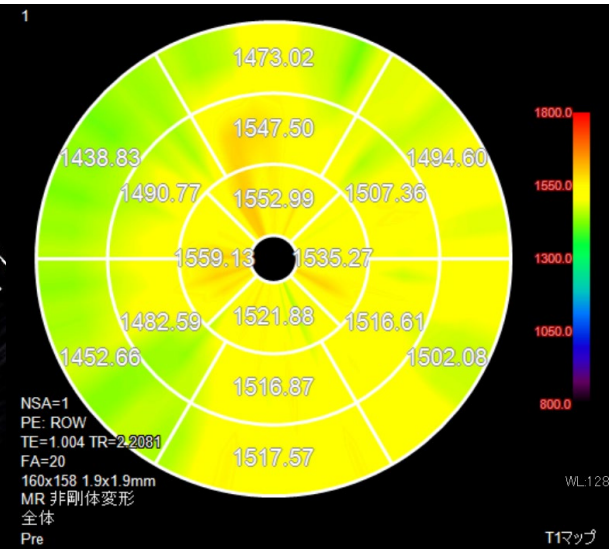

IVST : 16.1 mm
PWT : 16.2 mm

Native T1: 1506 ms

Hypertrophic Cardiomyopathy

Parasternal long-axis view

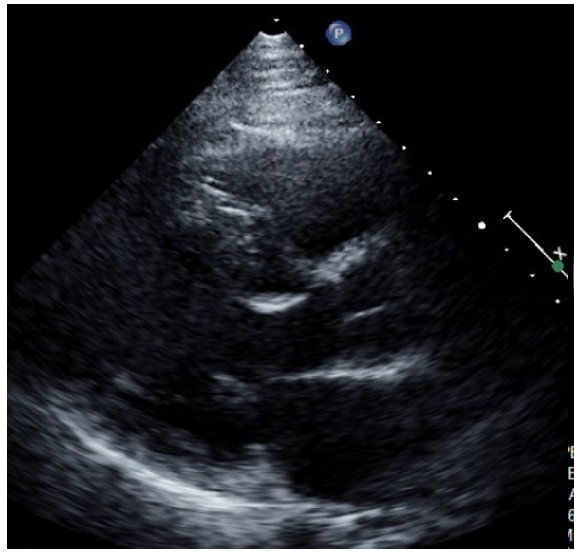

CMR T1 mapping

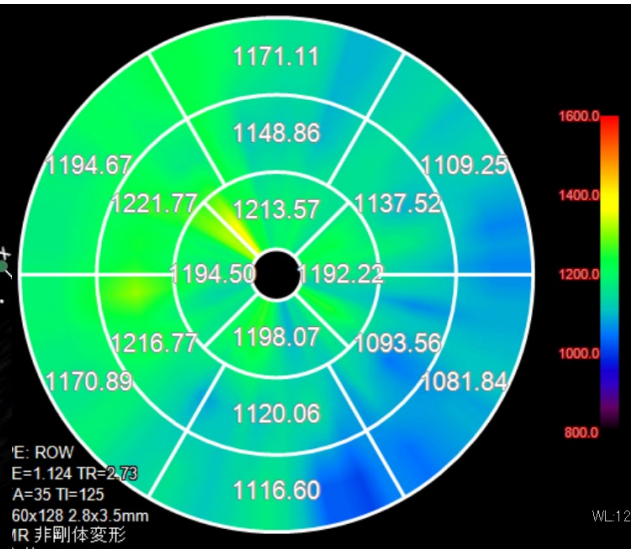

IVST : 16.8 mm
PWT : 9.2 mm

Native T1: 1168 ms

Figure 5

Essential Hypertension

Echocardiography

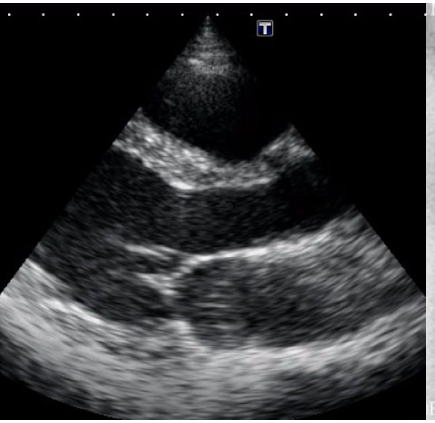

IVST : 12.8 mm
PWT : 12.2 mm

^{99m}Tc-PYP scintigraphy

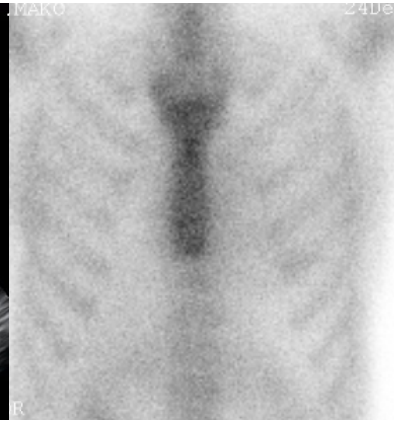

Grade 0

AL-CM

Echocardiography

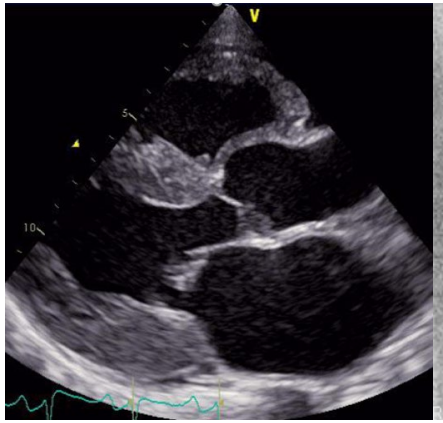

IVST : 20.1 mm
PWT : 19.1 mm

^{99m}Tc-PYP scintigraphy

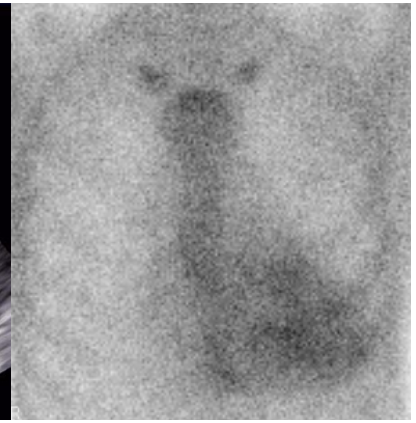

Grade 1

ATTRwt-CM

Echocardiography

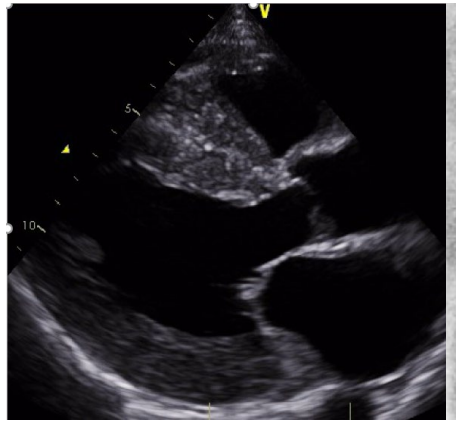

IVST : 17.2 mm
PWT : 18.8 mm

^{99m}Tc-PYP scintigraphy

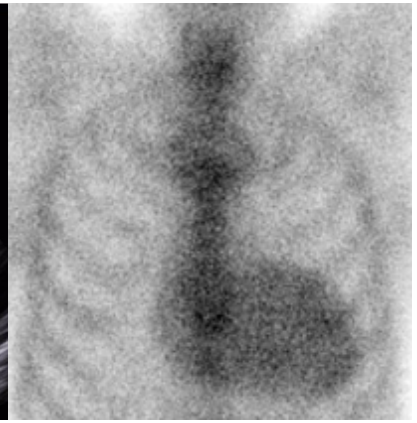

Grade 3

Figure 6

Echocardiography

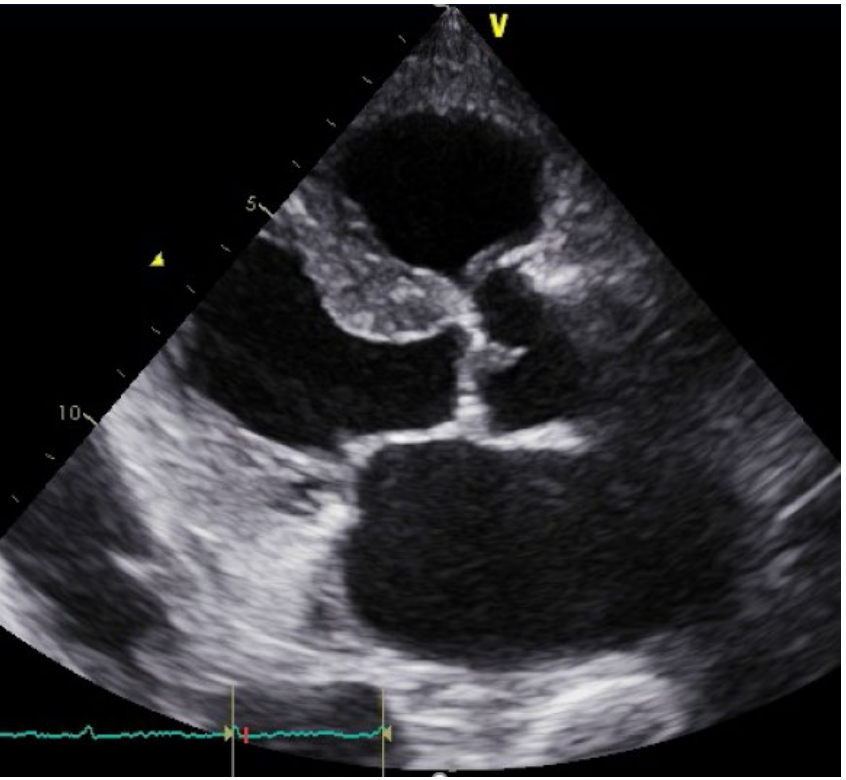

- IVST: 12.2 mm
- PWT: 13.0 mm
- LVEDV: 34 mL
- LVESV: 8 mL
- LVEF: 75 %
- LAVI: 65 mL/m^2

12-lead electrocardiogram

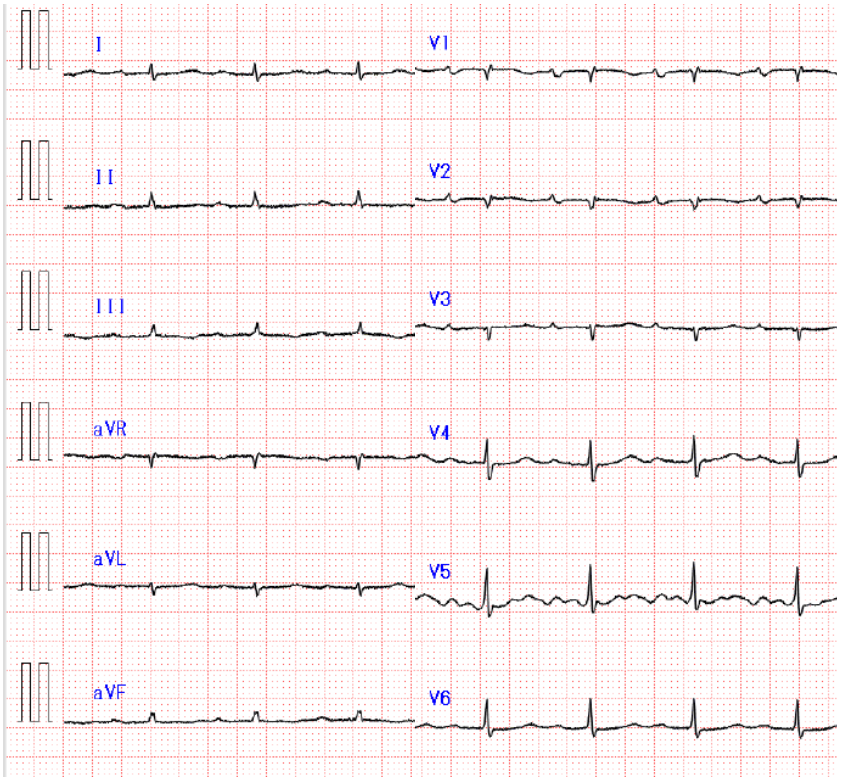

^{99m}Tc-PYP scintigraphy

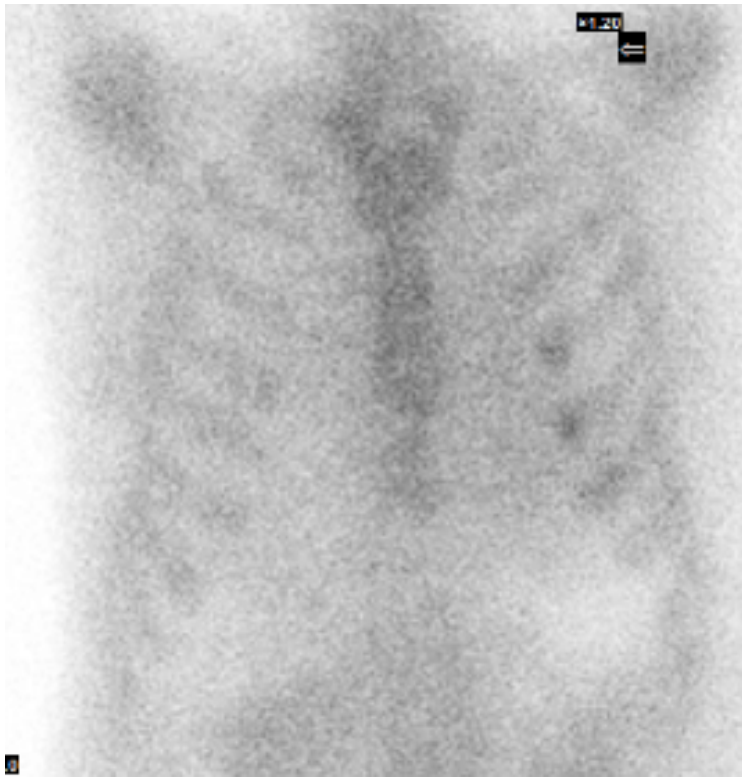

Grade 0

Figure 7

Echocardiography	Doppler-derived LV diastolic filling	Polar Plot Longitudinal Strain Mapping	^{99m}Tc-PYP scintigraphy
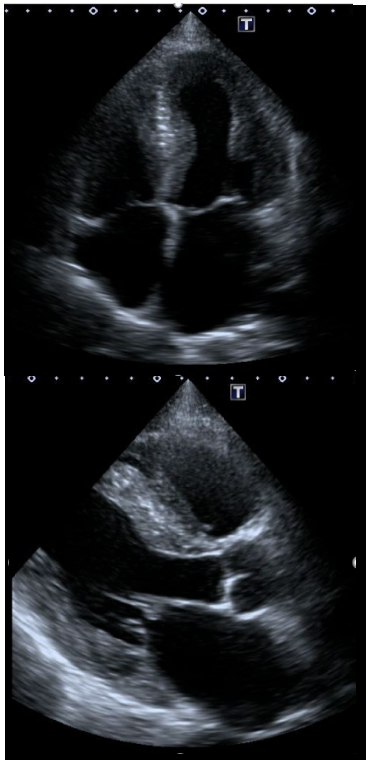	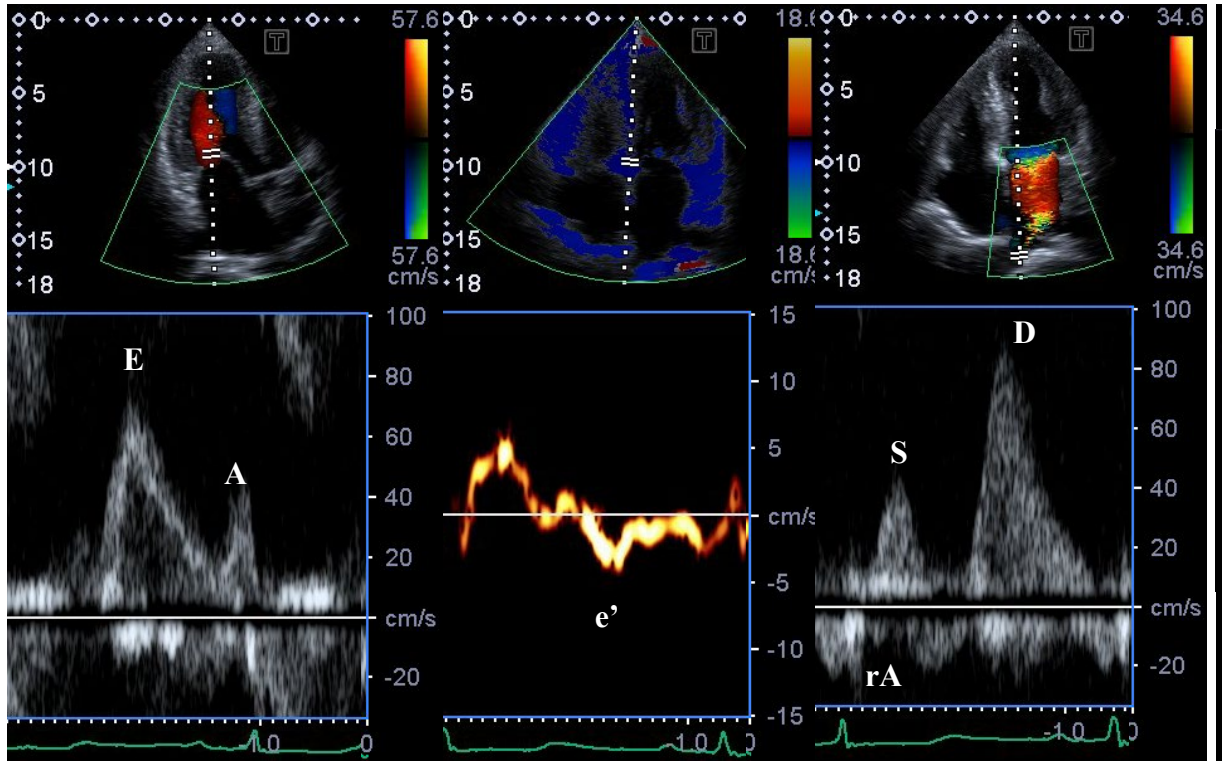	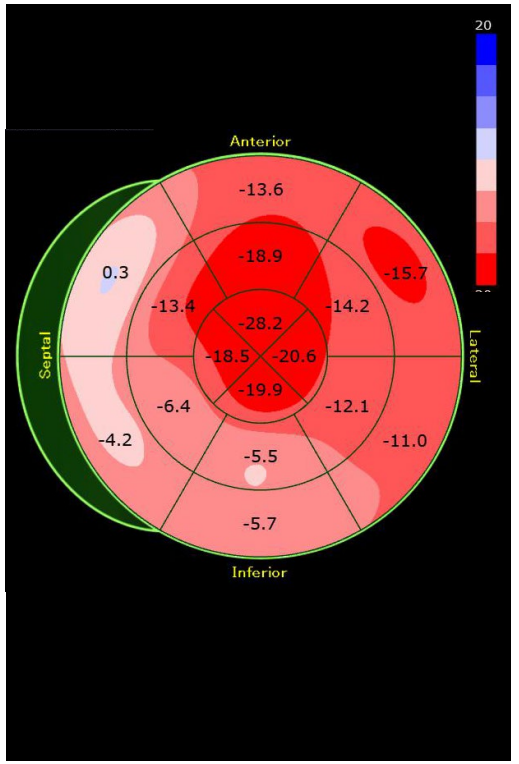	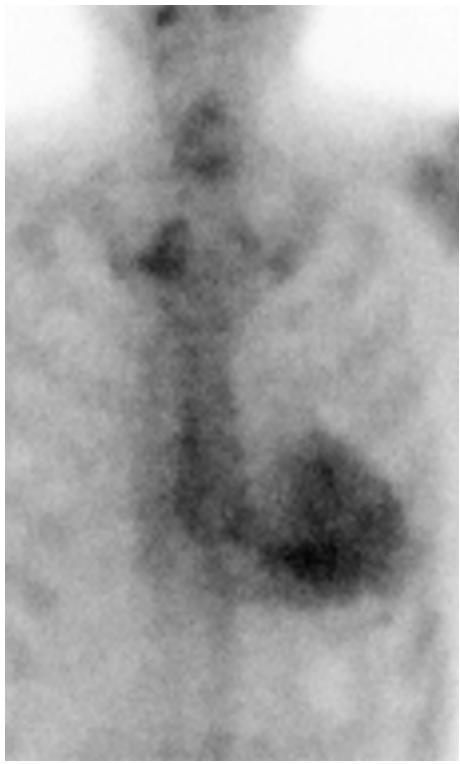
• IVST: 11.8 mm • PWT: 12.8 mm • LVEDV: 69 mL • LVESV: 22 mL • LVEF: 69% • LAVI: 42 mL/m^2	Grade III LV diastolic dysfunction	• GLS=13.0% • Relative apical longitudinal strain=1.08 • Septal apical-to-basal longitudinal strain=4.40	Grade 3

Figure 8

Echocardiography

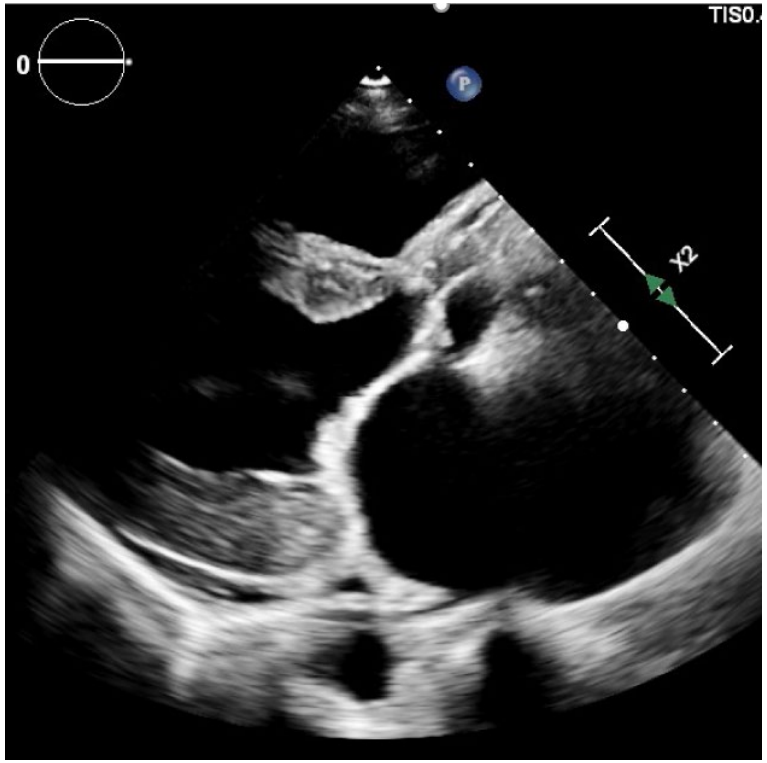

- IVST: 12.9 mm
- PWT: 16.0 mm
- LVEDV: 72 mL
- LVESV: 31 mL
- LVEF: 57%
- LAVI: 42 mL/m^2
- Peak V: 4.4 m/s
- Mean PG: 42 mmHg
- AVA: 0.70 cm^2

Polar Plot Longitudinal Strain Mapping

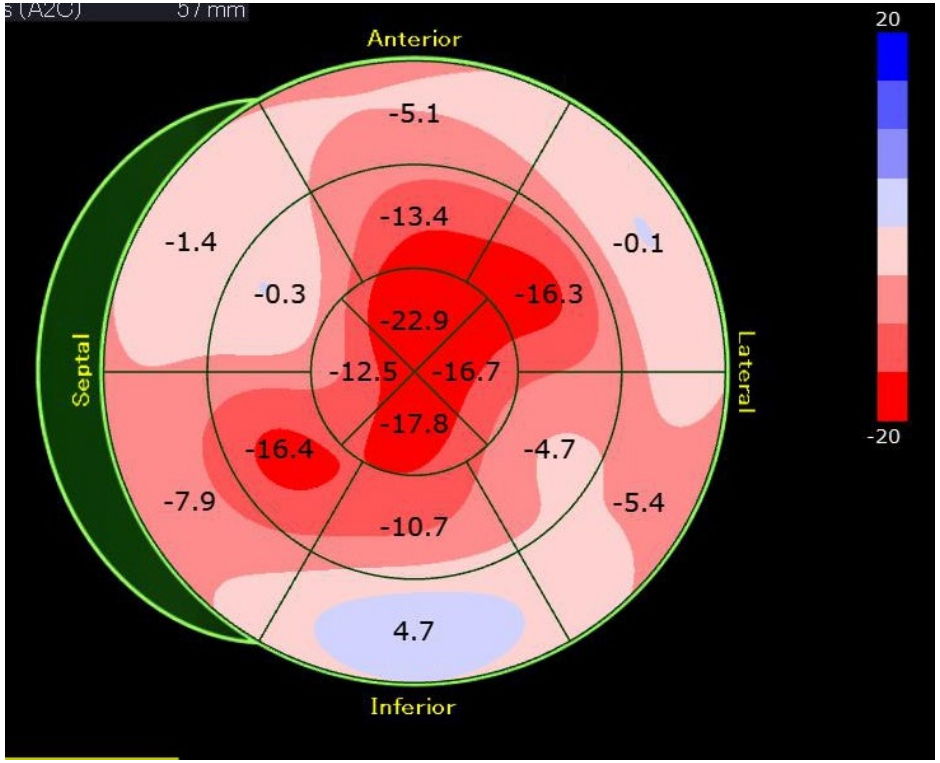

- GLS=9.8%
- Relative apical longitudinal strain=1.21
- Septal apical-to-basal longitudinal strain=8.93

^{99m}Tc-PYP scintigraphy

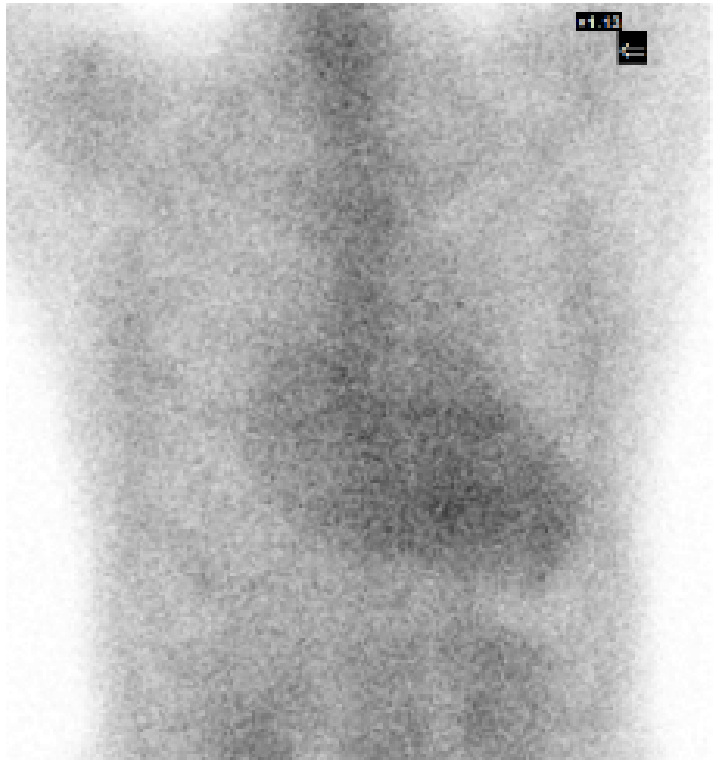

Grade 3

Figure 9

Echocardiography

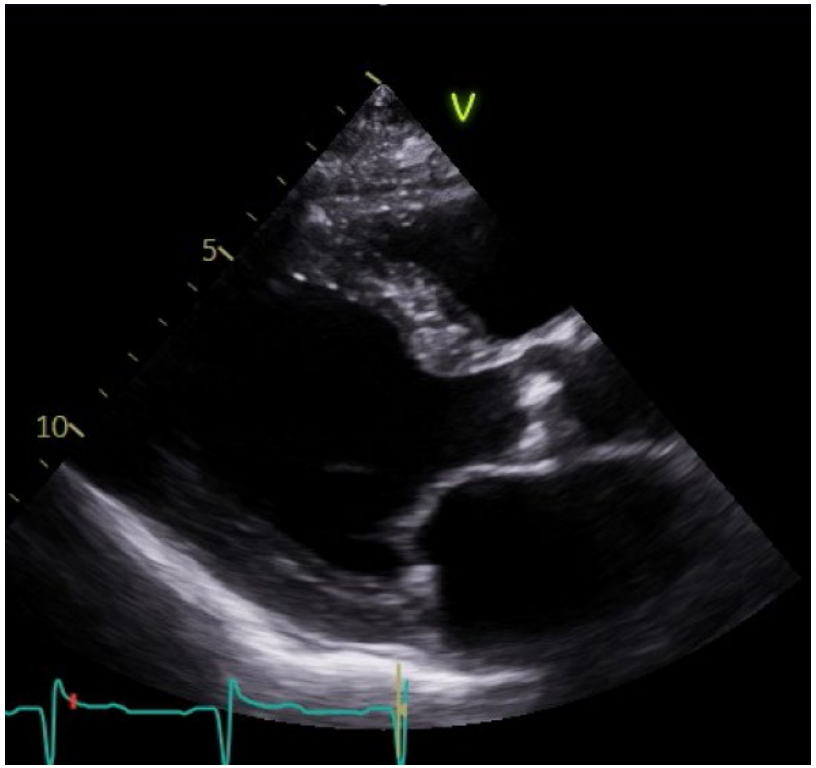

- IVST: 12.4 mm
- PWT: 12.7 mm
- LVEDV: 90 mL
- LVESV: 55 mL
- LVEF: 39%
- LAVI: 88 mL/m^2
- Peak V: 5.2 m/s
- Mean PG: 77 mmHg
- AVA: 0.36 cm^2

Cardiac CT

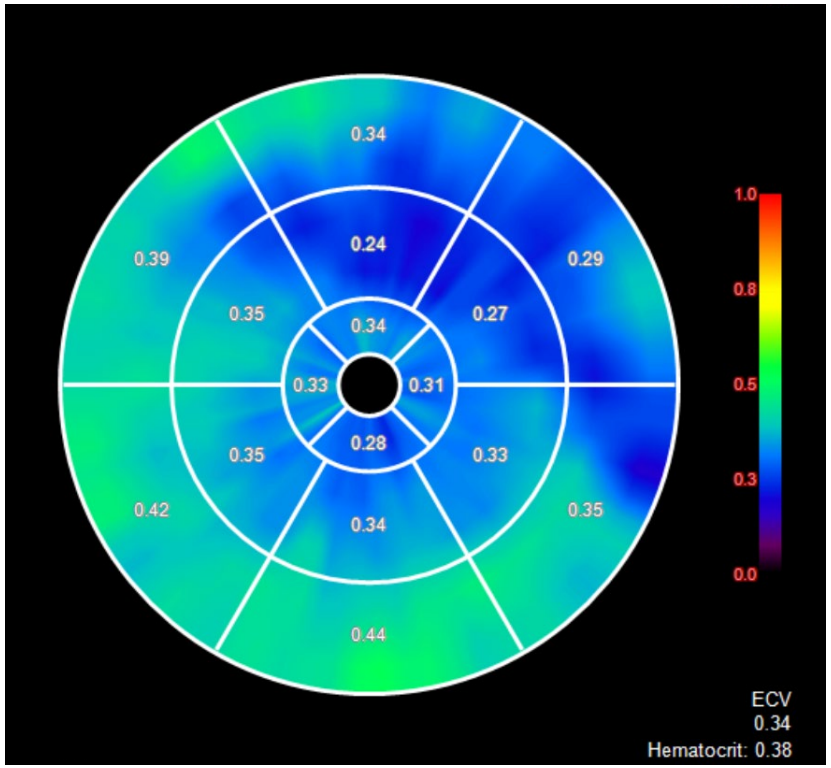

- ECV=34%

^{99m}Tc-PYP scintigraphy

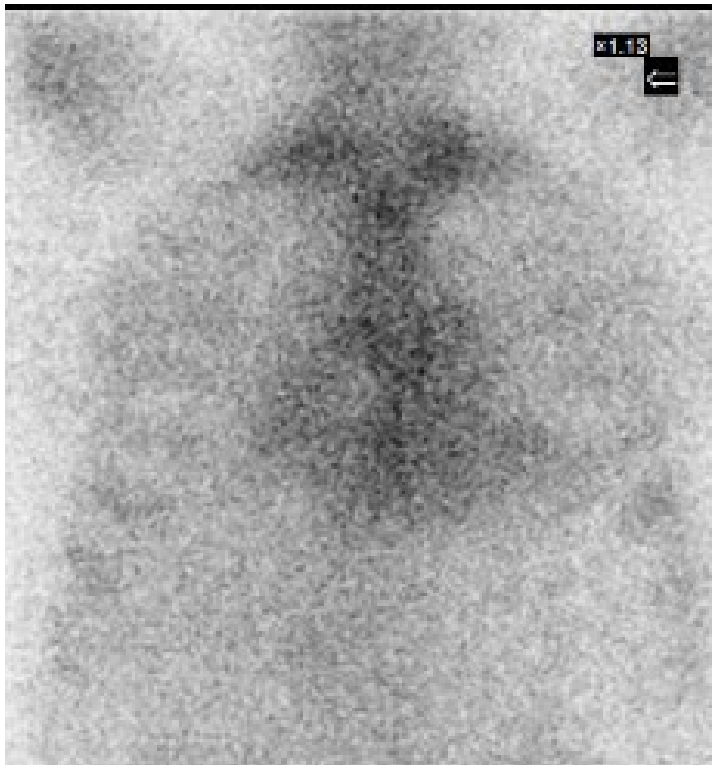

Grade 2